Colloids and Surfaces A: Physicochem. Eng. Aspects 516 (2017) 9–22

Contents lists available at ScienceDirect

Colloids and Surfaces A: Physicochemical and Engineering Aspects

journal homepage: www.elsevier.com/locate/colsurfa

Drop spreading and penetrating on micro/nano particle sintering porous with multiscale structure

Wolong Yang, Jinliang Xu*

The Beijing key Laboratory of Multiphase Flow and Heat Transfer for Low Grade Energy Conversion, North China Electric Power University, Beijing, 102206, PR China

HIGHLIGHTS

- Spreading on multiscale porous was investigated.
- Spreading on multiscale porous obeys the power law.
- Nano- roughness on particle surfaces accelerates drop spreading.
- Two modes of daughter drop generation were found.
- Inertia spreading dominates the first time daughter drop generation.

GRAPHICAL ABSTRACT

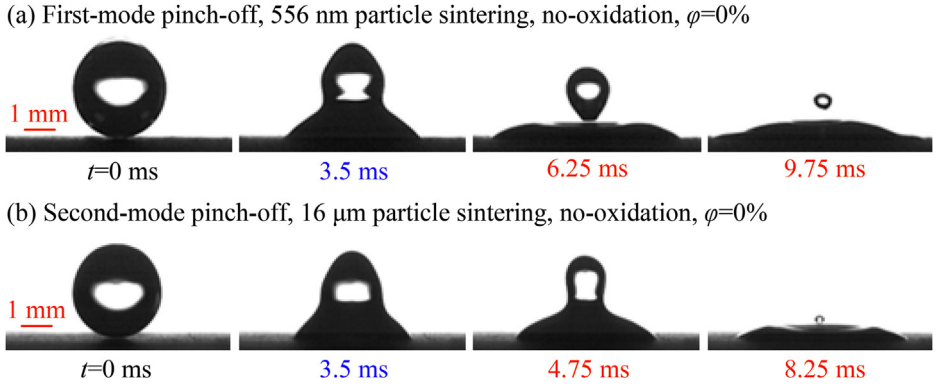

ARTICLE INFO

Article history:
Received 22 July 2016
Received in revised form 2 December 2016
Accepted 7 December 2016
Available online 8 December 2016

Keywords:
Multiscale porous
Wetting
Spreading
Penetration
Drop pinching-off

ABSTRACT

Drop spreading on micro/nano particle sintering porous is a challenge issue due to multiscale behavior. Here, the 556 nm or 16 μm copper powders are sintered with or without pore former, under vacuum or oxidation environment to generate twelve porous substrates, having two to three levels of length scales from nano to micron (10–100 μm). Drop spreading experiment was performed with careful data processing using time sequence images. It is found that early inertia drop spreading on porous surface follows the well-known power law. Nano-roughness increases wettability to increase the power-law coefficient C to accelerate spreading for both nano and micro-particle sintering surfaces. The porosity does not change the power law exponent α for nano-particle sintering surface, but the increased porosity decreases both C and α for micro-particle sintering surfaces. Nano-particle sintering porous lasts longer duration time of inertia dominant spreading, during which the first time daughter drop emission is success. Micro-particle sintering porous shortens the duration time. The pinching neck is still thick at the end of the duration time. Thus, the first time daughter drop emission is not success. This work identified the necessary condition for the first time daughter drop generation is that the pinching phenomenon should occur during the inertia dominant spreading stage. Spreading, capillary wave and penetration are competition mechanisms to form the S-shape pinching neck heights. The re-increase of the neck heights evidences the secondary capillary wave propagation, corresponding to the second time daughter drop emission. The secondary daughter drop

* Corresponding author.
E-mail address: xjl@ncepu.edu.cn (J. Xu).

http://dx.doi.org/10.1016/j.colsurfa.2016.12.005

emission time (t_{SP}) is either shorter or longer than the maximum spreading diameter time t_M, inferring that the secondary daughter drop generation is not related to the porous structure.

1. Introduction

We investigate slow drop deposition and spreading on micro/nano particle sintering porous surface. The daughter drop pinch-off and breakup were also paid great attention. To the authors' knowledge, spreading on such multiscale complicated surface is not reported previously [1–24]. This section shortly reviewed the accumulated knowledge regarding this topic. Articles dealing with drop impacting with higher impacting velocities on various surfaces are beyond the scope of this paper.

Liquid drop spreading on solid plate and porous surface widely happen in nature and engineering [12–18]. Table 1 summarizes articles dealing with slow drop deposition and spreading. Generally, three types of problems are studied: (1) spreading on solid plates without holes [1–9], (2) spreading on porous surfaces with uniform pore structure [10–22], and (3) drop–drop or drop-liquid pool coalescence induced deposition or spreading [23,24]. Early studies on drop spreading on solid surfaces only considered the viscous dominant spreading [25]. Now, we recognize that the early inertia dominant stage lasts ~ms timescale, followed by the viscous dominant stage. Biance et al. [1] experimentally determined the inertia spreading diameter D_t obeying the power law of $D_t \sim t^{0.5}$ on complete wetting glass surface using initial water drop diameter of $D_0 = 2.0$ mm. Later, many studies were reported on such problem, including surfaces with changed wettability [3,5,8], soft surfaces [4,7]. It is concluded that the early inertia dominant spreading obeys the power law of $D_t = Ct\alpha$, noting that C and α are dependent on surface wettability, and α may be deviating from 0.5.

The spreading becomes more complicated when slow drop deposits on a porous surface. In addition to the spreading on the horizontal plane, penetration inside porous medium affects the spreading. Davis & Hocking [10,11] presented theoretical studies by the lubrication approximation theory with drop deposition on uniform porous medium, not considering wettability. Starov et al. [12–14] performed theoretical studies by Brinkman's equation and lubrication theory, assuming spherical drop. They did not consider the inertia dominant spreading but focused on the viscous spreading, obeying $D_t \sim t^{0.1}$. Clarke et al. [15] investigated drop deposition on thin micro-porous filter membranes. The spreading and penetration are described by molecular dynamics and Darcy law. The predictions agree with the measured contact angles. Frank & Perre [18,21] performed Lattice Boltzman simulation, showing that the early spreading follows power law with exponent and prefactor decreasing with increasing porosity.

When drops were deposited gently, they rested on the surface until the interstitial air layer was drained [23]. The two liquid masses then touched to form a thin liquid bridge that rapidly widened, sending capillary waves racing up the drop surface. As the drop drained into the reservoir, its shape generally evolved into a cylindrical column with a height greater than that of the initial drop. The neck then narrowed due to the inward pull of surface tension, pinched off to form a daughter droplet with a radius approximately half that of the initial drop. The coalescence process is controlled by a competition between the vertical and horizontal rates of collapse, both of which are driven by surface tension. Zhang et al. [24] identified the critical diameter ratio of two drops, above which a satellite is produced during their coalescence. The critical parent ratio is as small as 1.55. However, they identified novel pinch-off

Nomenclature

C	The power-law prefactor
D_0	Initial diameter of droplet, m
d_m	Mean particle diameter, m
D_{max}	Maximum spreading diameter, m
d_p	Particle diameter, m
D_t	Spreading diameter, m
FP	First time drop pinching-off
t	Time, s
H	Distance between droplet bottom and porous surface, m
h_t	Neck height, m
H_t	Drop height, m
I	Inertia dominant spreading
K	Permeability, m2
La	Laplace number
M	Micro-porous
MR	Micro-porous with nano-roughness on particles
MS	Micro-porous with smooth particle surface
NR	Nano-porous with nano-roughness on particles
NS	Nano-porous with smooth particle surface
r	Roughness factor
S	Shape coefficient
t	Time, s
t_{FP}	the time at the first time drop pinching-off, s
$t_{h_t}(\max)$	the time at the maximum neck height, s
$t_{H_t}(\max)$	the time at the maximum drop height, s
t_I	the duration time of inertia dominant spreading, s
t_M	the time at the maximum spreading diameter, s
t_p	Penetration time, s
t_{SP}	the time at the second time drop pinching-off
We	Weber number
v	Velocity, m/s

Greek symbols

α	the power-law exponent
β_{max}	Maximum spreading factor
ε	Porosity
θ	Contact angle between liquid and solid surface, °
θ_w	Contact angle between liquid and microstructure, °
μ	Viscosity, Pa s
ρ	Density, kg/m3
σ	Surface tension force, N/m
φ	Volume concentration of pore former
τ	Inertia time scale, s

Subscript

cw	Capillary wave
g	Gas
l	Liquid
pe	Penetration
s	Solid
sp	Spreading

Table 1
The spreading or daughter drop generation studies in the literature.

References	Surface	Fluid	Research methods	Findings and comments
Biance et al. [1]	Completely hydrophilic glass plate	water drop with D_0 = 2 mm	Experimental study with slow drop deposition on surface	Showing early inertia dominant spreading with $D_t \sim t^{0.5}$
Rioboo et al. [2]	Similar to [1]	Water and other fluids with multi-drop diameters	Experimental study with slow drop deposition, focusing on daughter drop pinch-off	The drop pinch-off is possible at higher position of the center of drop mass.
Bird et al. [3]	Modified silicon surface from hydrophilic to hydrophobic	Three water-glycerol solutions with D_0 = 1 mm	Experimental study on slow drop deposition, focusing on effect of surface wettability on spreading	Early spreading obeys the power law with C and α depending on contact angles
Winkels et al. [5]	Surfaces with four contact angles for MD simulation and with three contact angles for experiment	Lennard-Jones liquid of D_0 = 60 nm for MD and D_0 = 1 mm for experiment	Focusing on very short time of <0.1 ms drop deposition and spreading	Early spreading follows $D_t \sim t^{0.5}$ with constant α and increased C by increasing surface wettability.
Ding et al. [6]	Glass plate with various contact angles	Water, acetone, methanol and other mixture fluids	Experimental study on first and second stage drop pinch-off and numerical simulation	Find the first and second stage drop pinch-off and identify the capillary wave mechanism
Chen et al. [7]	Five soft viscoelastic plates and a hard hydrophobic glass plate	Water and water/ethanol mixture with D_0 = 2 mm	Focusing on transition from inertia spreading to viscoelastic stage	Inertia spreading obeys $r = Ct^{\alpha}$ and developed a mode for transition from inertia spreading to viscoelastic spreading
Sun et al. [9]	Glass plate with five contact angles	Water drop of 2 mm	Experimental measurement	Very small drop ejection due to ultra-fast spreading
Davis & Hocking. [10,11]	Uniform pore not considering wettability	General fluid	Theoretical study based on lubrication approximation theory	Several models were considered that involve the competition between spreading and imbibition by a permeable substrate
Starov et al. [12–14]	Thin and thick quasi-uniform porous membrane	Silicon oil with viscosities of 0.554P, 1.18P and 5.582P	Theoretical study using Brinkman equation [12] and lubrication theory [13], assuming spherical drop, experimental study on slow drop deposition	Not considering inertia dominant spreading but focusing on viscous dominant spreading which obeys $D_t \sim t^{0.1}$. Competition between spreading and penetration exists.
Clarke et al. [15]	Thin microporous filter membranes made from mixed cellulose esters with pore size from 0.1-0.8 μm	Water, aqueous solution of glycerol and hexelene glycol)	Spreading and penetration are described by MD simulation and Darcy law	The predictions agree with the measured dynamic contact angle and spreading diameter
Alleborn & Raszillier. [16]	Two homogeneous anisotropic layers	Ideal incompressible liquid	Numerical simulation and lubrication approximation analysis	Effect of permeability of two layers of membranes on spreading and penetration were identified.
Haidara et al. [17]	Nanoporous alumina membranes with 60 μm thickness and isolated pores	PDMS oil with volume of 3–4 μl	Slow drop position	In the viscous dominant regime, spreading obeys the Tanner law of $D_t \sim t^{0.1}$, spreading velocity obeys $v \sim \eta^{-n}$, where n = 0.55.
Frank and Perré. [18,21]	Six surfaces including solid plates and uniform porous surfaces	General liquid	Lattice Bolzman numerical simulation	Early spreading follows power law with exponent and prefactor decreasing with increasing porosity.
Ding & Theofanous. [19]	Single or multi capillary tubes	Using different Re and We	Numerical simulation with Navier-Stokes equations and diffuse-interface method	Small drop breakup happens either in or outside of capillary tube, related to inertia force
Shuai et al. [20]	Solid plates and porous medium (uniform pore)	General fluid	Numerical simulation and smoothed particle hydrodynamics	Early spreading still obeys power law. Gravity force has no effect on inertia spreading
Lee et al. [22]	Natural porous stone	Water, 25 °C and D_0 = 2 mm	Experimental study with impacting velocity of 0.2–4 m/s, We = 1–440 and Re = 400–8000	Dynamic contact angles increase then decrease due to an air layer between liquid and stone. The spreading stops when air lay was broken. The maximum contact angle is larger with larger porosity.
Blanchette & Bigioni. [23]	Liquid pool	Ethanol drop with r = 0.535 mm	Numerical simulation with Navier-stokes equation and Oh = 0.11	The drop pinch-off depends on the capillary wave reaching the drop summit. A critical Oh exists beyond which drop pinch-off does not appear.
Zhang et al. [24]	Various drop sizes	Distilled water and glycerin/water mixtures	Experimental study on coalescence of drops with different sizes with Bo < 0.1	Two types of daughter drop pinch-off if size ratio of two drops larger than 1.55

Table 2
Parameters of the four types of porous samples.

porous		d_m	φ	Oxidation (Yes/No)	ε
NS	NS(0)	556 nm	0	N	26.22%
	NS(0.2)		0.2		40.97%
	NS(0.4)		0.4		50.02%
NR	NR(0)	556 nm	0	Y	20.84%
	NR(0.2)		0.2		34.68%
	NR(0.4)		0.4		44.97%
MS	MS(0)	16 μm	0	N	37.54%
	MS(0.2)		0.2		58.03%
	MS(0.4)		0.4		73.22%
MR	MR(0)	16 μm	0	Y	35.39%
	MR(0.2)		0.2		56.89%
	MR(0.4)		0.4		71.02%

Note: φ = 0, 0.2 and 0.4 means that the pore former volume concentration is 0, 0.2 and 0.4, respectively, ε is the porosity.

dynamics close to the critical size ratio, where the satellite does not fully separate, but rather goes directly into a second stage of the coalescence cascade, thus generating a much smaller satellite droplet.

We deal with drop spreading on particle sintering porous surface. Particle sintering technique has been widely used in metallurgy industry for various applications [26]. In heat exchangers and heat pipes, particle sintering layer on high heat flux surface enhances heat transfer. If a porous medium with uniform pore size is used, strong conflicts exist because different process requires different pore size. For example, smaller pores are helpful for capillary pressure generation but larger pores are needed for liquid suction and vapor venting. Porous medium with non-uniform pores is required to satisfy these requirements [27]. When liquid drops contact the multiscale porous surface, a lot of issues are unknown. For example, does the early spreading follow the power law? How long is the duration time of the inertia dominant stage? Does the daughter drop ejection happen? What is the connection between inertia dominant spreading and daughter drop generation? This paper performed experiments to answer the above questions.

2. Materials and methods

2.1. The porous structure fabrication and characterization

We used hydrophilic copper powders with average particle diameters of d_m = 556 nm and 16 μm. The two types of particles were carefully selected and had narrow ranges of 200–900 nm and 10–30 μm, respectively. The purity of copper powders was 99.6%. Sintering particles in the oven forms smooth particle surfaces under the vacuum environment, and nano-roughness on particle surfaces under the oxidation environment. The element concentration analysis indicates the perfect copper element for vacuum sintering and copper oxide (CuO) on particle surfaces for oxidation sintering. In order to generate different porosities in porous wick, the copper powders were thoroughly mixed with Na_2CO_3 powders (pore former). Then, the mixture powders were sintered in the oven. Deionized water flushed the fabricated porous to remove the residual substance. The porous sample was ready for use after drying.

Table 2 lists the porous samples, in which letters N, M, S and R represent nano-particle, micro-particle, smooth particle and rough surface particle. Thus, NS and NR mean the nano-particle sintering with smooth particle surface and nano-roughness on particles, respectively. Each family of porous sample contains three porosities with different pore former (Na_2CO_3) volume concentrations of φ = 0, 20% and 40%. The volume concentration was converted to weight concentration so that the copper powders and pore former were accurately weighted by an electronic balance with an uncertainty of 0.001 g. The porosity was measured by the Archimedes principle, having the uncertainty of less than 1%. The porosities are increased by increasing the volume concentrations of pore former. The nano-roughness on particle surface decreases porosity. The sintering samples of nano-particles and micro-particles had the porosities in the range of 20–50%, and 35–73%, respectively. The porous samples had an overall diameter of 20.0 mm and a thickness of 2.0 mm.

Fig. 1 shows the 556 nm-particle sintering without pore former. Fig. 1a–c illustrates porous with smooth particle surface. The pore network contains pores and pore channels. The pore is formed by sintering three particles together. Assuming equal particle sizes, the pore diameter equals to $0.21d_p$ [28], where d_p is the particle diameter. Pore channel is automatically formed even there is no pore former. It can be longer or shorter with its width of $\sim d_p$. Fig. 1d–f shows the oxidation formed nano-floss on particle surfaces. Single nano-particle was difficult to be observed because the nano-structure was covered on the particle surface.

Fig. 2 shows the 16 μm particle sintering. The MS(0) sample also contains pores and pore channels (Fig. 2a–c). The oxidation forms nano-crystals on particle surfaces (Fig. 2f). Single particle can be easily identified due to larger particle size. Fig. 3 shows the effect of pore former contents on the porous structure. Under the condition of pore former contents of 20% and 40%, larger pore cavities are seen.

Figs. 1–3 demonstrate multiscale characteristic. For particle sintering without oxidation, two size levels can be seen: pore size of $0.21d_p$ and pore channel with its width of $\sim d_p$. For particle sintering with oxidation, three size levels can be seen: pore size of $0.21d_p$, pore channel with its width of $\sim d_p$, and nano-scale roughness. When the sintering is performed with pore former, pore channels are replaced by larger pore cavities, having the size of 10–100 μm.

2.2. The droplet deposition experiment

Fig. 4 shows the experimental facility. The droplet was generated by a micro-injector controlled by a computer. The droplet was gently deposited on the porous surface. The droplet dynamics was captured by a high speed camera adapted with a microscope. The light-emitting-diode (LED) was used as the light source. The image recording rate was 4000 frames per second. The image covered the size of 512 pixels by 512 pixels. Correspondingly, the size resolution was 15.6 μm per pixel.

The physical properties of water at the room temperature are ρ = 998.2 kg/m^3 (density), $\mu = 1.005 \times 10^{-3}$ Pa s (viscosity) and $\sigma = 72.75 \times 10^{-3}$ N/m (surface tension force). During experiment, the droplet bottom has a short distance of about H = 0.6 mm to the porous surface. Thus, the impacting velocity on the porous surface is estimated to be 0.12 m/s, at which the Weber number for the drop impacting is $We = \rho v^2 D_0/\sigma \leq 0.31$. The present work investigates the slow drop deposition problem. The droplet diameter before deposition was D_0 = 1.92 mm.

The obtained video images were carefully processed, including dynamic spreading diameter (D_t), maximum spreading diameter (D_{max}), drop total height (H_t) and pinching neck height (h_t). The time t = 0 is defined as the moment just before the drop contacts the porous surface. Four specific state points are paid attention. The point I is the beginning of the spreading diameter deviating from the power law expression. The time t_{FP}, t_{SP} and t_M are the time at which the first time drop pinching-off, second time drop pinching-off and maximum spreading diameter appear, respectively.

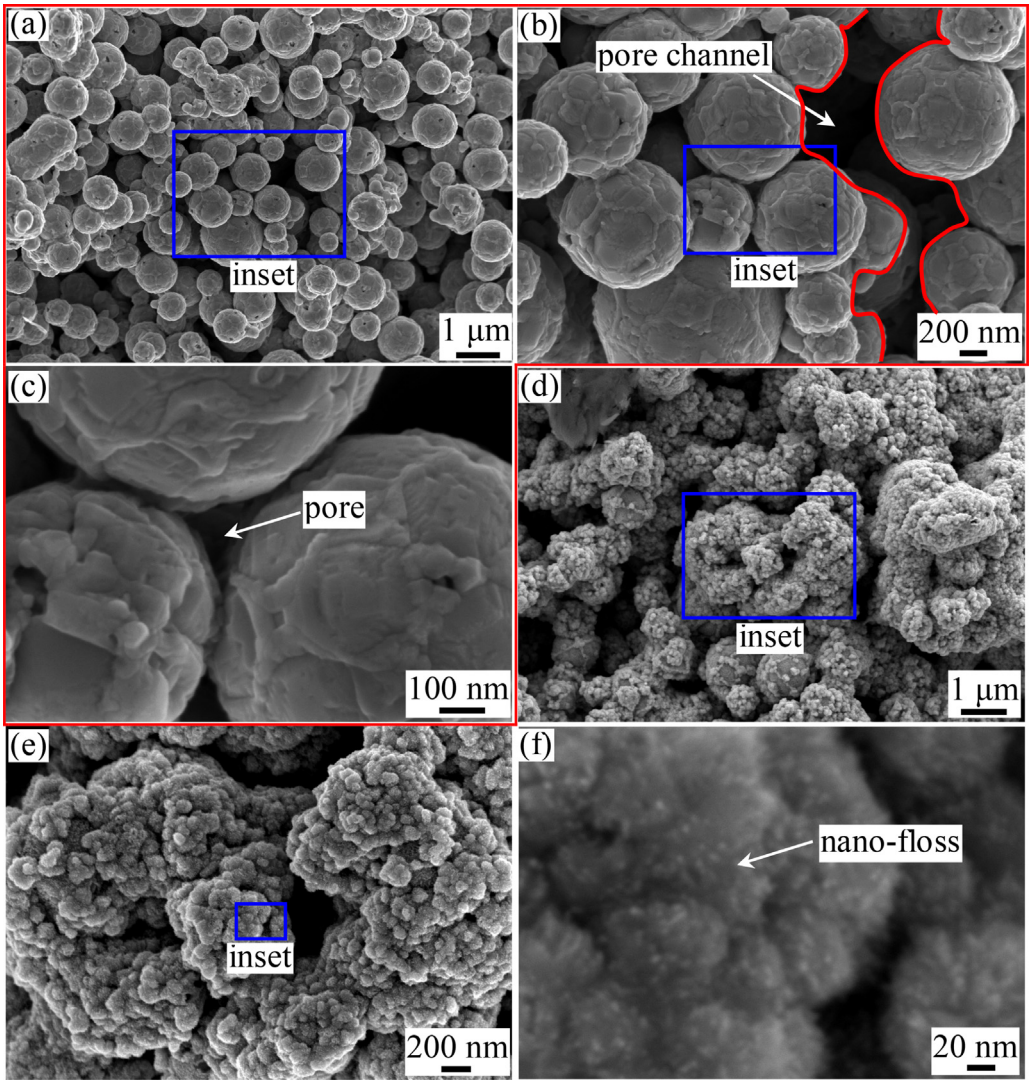

Fig. 1. SEM images for 556 nm particle sintering porous (a–c for NS(0); d–f for NR(0)).

3. Results and discussion

3.1. General characteristic of droplet spreading and penetration

We found two modes of daughter drop pinch-off: the first mode pinch-off for nano-particle sintering (NS and NR samples), and second mode pinch-off for micro-particle sintering (MS and MR samples). Fig. 5 shows the sequence video images (Fig. 5a for NS(0) sample) and shape curves for NS(0), NS(0.4), NR(0) and NR(0.4). The phenomena are similar for these samples. Four typical shapes are marked at specific time. The green, blue, dashed black and red curves refer as the first time daughter droplet emission, ending of inertia dominant spreading, second time daughter drop emission, and maximum spreading diameter, respectively.

Fig. 5a–b shows images and shapes for 556 nano-particle sintering with smooth particle surface and without pore former. When a mother drop contacts the hydrophilic porous surface, it will sharply spread in several milliseconds. The drop can be divided into a top part and a bottom part, connected by a neck (see t = 1–6 ms). A small daughter drop of about 0.8 mm was thoroughly pinched off at t = 6.25 ms (first time pinch-off). The inertia dominant spreading happened during t = 0–8.25 ms. Section 3.2 gives how to determine the inertia dominant spreading. The first time ejected daughter drop fell down and contacted its mother drop at about t = 7 ms. A very small drop of about 0.3 mm was emitted at t = 9.75 ms (second time drop pinch-off). Then, the base drop attained maximum spreading diameter at t = 10.0 ms. The drop receding process was followed for t > 10.0 ms. The liquid was thoroughly penetrated inside porous wick at t = 95 ms. Fig. 5b–e shows the effect of particle surface roughness and porosity on droplet dynamics, which is analyzed in Sections 3.2 and 3.3.

Fig. 6 shows pictures and shapes on micro-particle sintering material. Compared with nano-particle sintering material, the first time daughter droplet ejection does not happen for micro-particle sintering porous. Instead, only a very small daughter droplet is pinched off at specific time. Fig. 6a–b shows pictures for MS (0) with smooth particle surface and zero pore former concentration. The inertia dominant regime lasts during t = 0–4.75 ms. Even though a thick neck was observed during t = 6.25–6.50 ms, the top part of droplet did not pinched off. The lifting part of droplet falls down and merges with the base part of droplet, yielding a very small droplet of about 0.15 mm pinching-off at t = 8.0 ms (the second time drop pinch-off).

Fig. 7a–b shows spreading diameter D_t. For 556 nm particle sintering porous, the nano-modification on particle surfaces accelerates drop spreading before D_{max}. The early spreading is

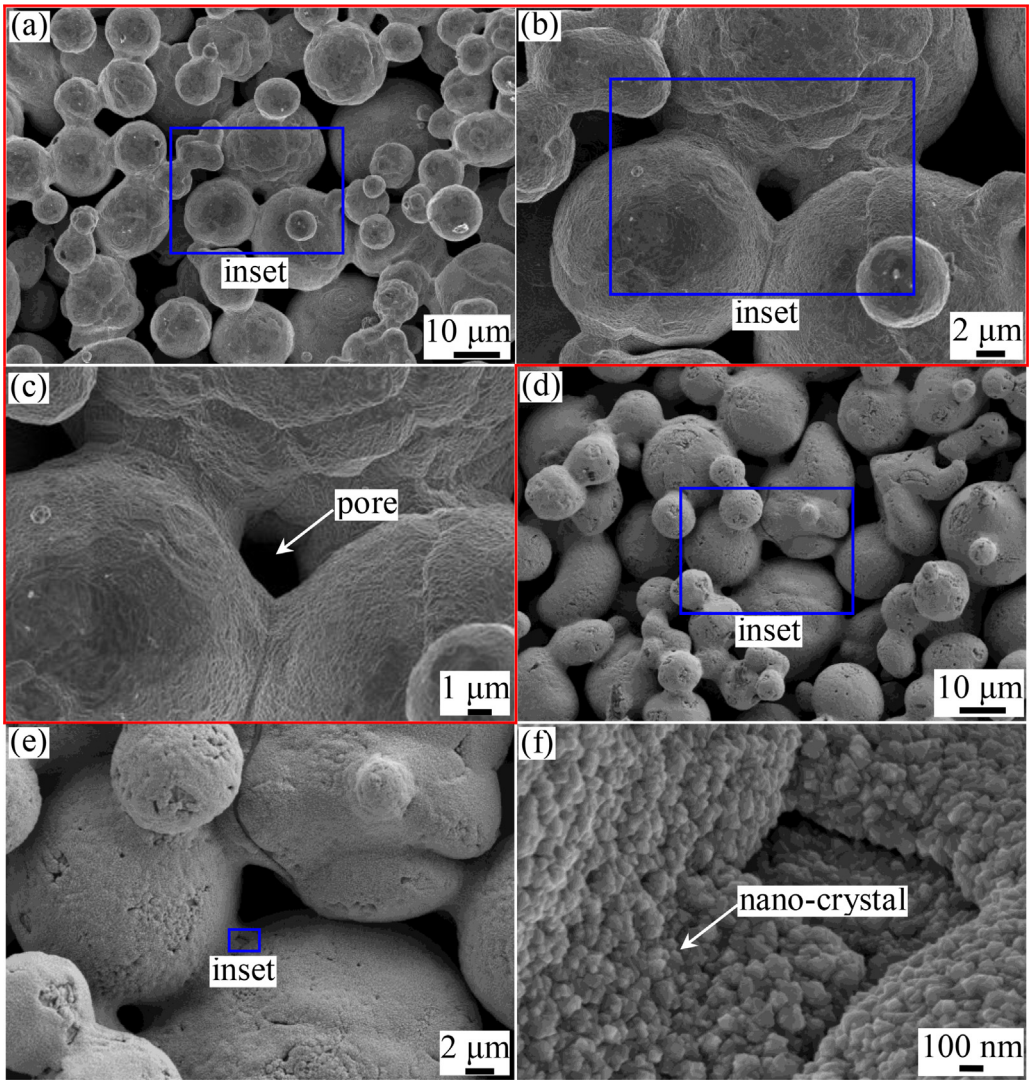

Fig. 2. SEM images for micro-particle sintering porous (a–c for MS(0); d–f for MR(0)).

mainly competed by capillary and inertia forces. Nano-modification increases wettability to enhance the driving force for spreading. However, at the same porosity, nano-modification extends the whole penetration time, due to the partial block effect by the nano-scale roughness on nano-particle surfaces to increase the viscosity resistance. Porosity does not influence D_t before D_{max}, indicating the unimportance of penetration in porous wick. Porosity apparently influences droplet receding beyond D_{max}. Larger pore former concentration significantly shortens the penetration time, due to the increased pore cavities to reduce viscosity resistance.

For 16 μm particle sintering porous, nano-roughness on particle surfaces accelerates spreading before D_{max} at the same porosity, similar to that for nano-particle sintering. But it does not influence droplet receding and the whole penetration time. This is because the nano-roughness has much smaller size compared with micro pore network. The viscosity resistance in porous wick is mainly relied on the micro pore network. Porosity influences both droplet spreading and receding.

The effect of particle size and porosity on droplet penetration in porous wick can be explained by the Kozeny-Carman equation [29]:

$$K = \frac{d_m^2 \varepsilon^2}{S(1-\varepsilon)^2} \quad (1)$$

where K is the permeability, d_m and ε are the particle diameter and porosity, respectively. S is the shape coefficient, which can be 180 [29]. The larger K, the faster the liquid penetration in porous is.

Equation (1) shows the relationship between K and ε as $K \sim \left[\frac{\varepsilon}{1-\varepsilon}\right]^2$, having faster increasing speed than ε^2. K has a square law of $K \sim d_m^2$. For 556 nm particle sintering porous, K at the pore former concentration of 40% is 7.9 times of that at the zero pore former concentration. Alternatively, at the same pore former concentration of 40%, K for 556 nm particle sintering porous is only 0.016% of that for 16 μm particle sintering porous. This analysis explains the data trend shown in Fig. 7.

Equation (1) explains Fig. 7c, in which the penetration time t_p is decreased with increasing porosity. This trend is more obvious for nano-particle sintering porous (NR and NS samples), in which pore cavity size is ultra small if pore former was not used. Correspondingly, $\beta_{max} = D_{max}/D_0$, where D_{max} and D_0 are the maximum spreading diameter and initial drop diameter, is decreased with increasing porosities (see Fig. 7d).

3.2. The early inertia dominant spreading

Few studies were reported on the early inertia dominant spreading on porous surface. Frank and Perre [18] presented numerical

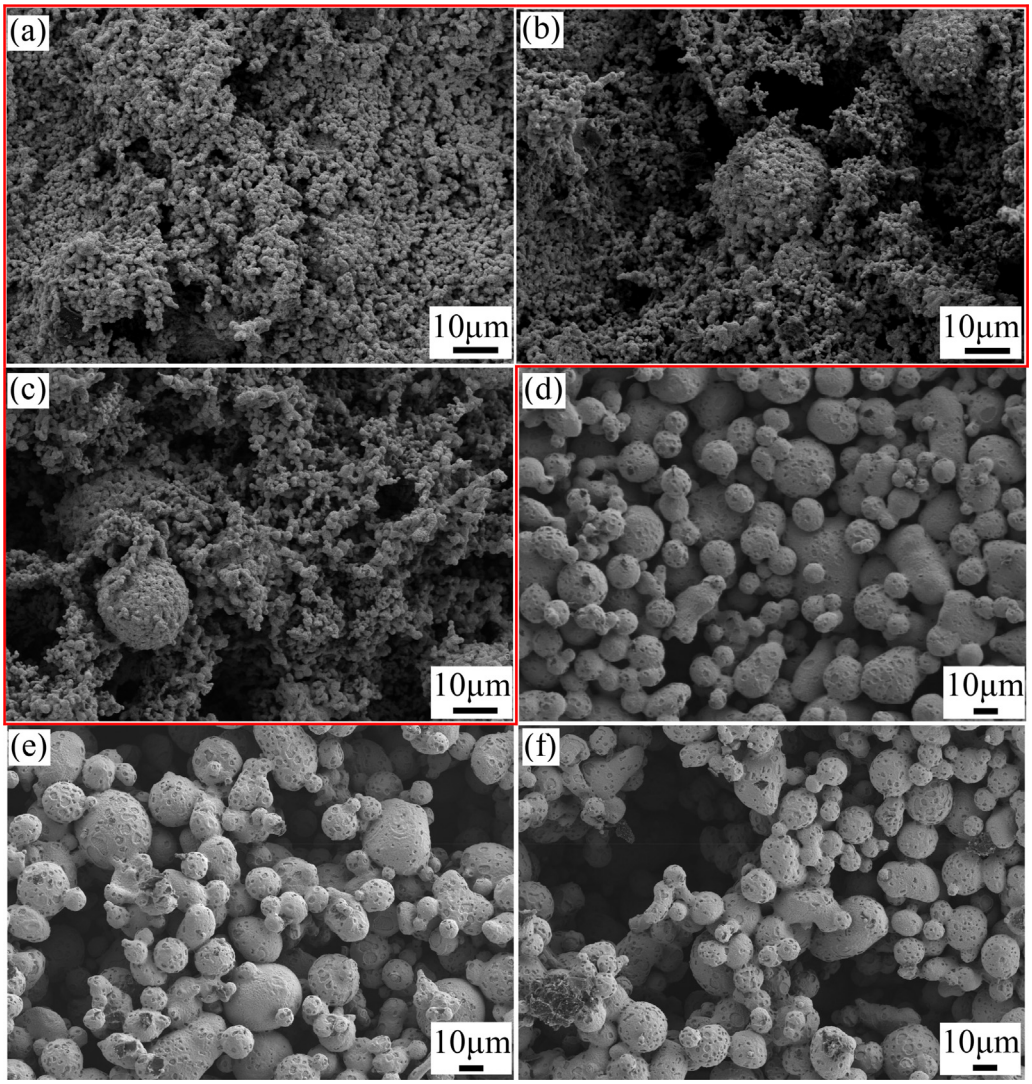

Fig. 3. Effect of porosity on porous structure (a for NR(0); b for NR(0.2); c for NR(0.4); d for MR(0); e for MR(0.2); f for MR(0.4)).

simulation of drop spreading and capillary absorption on a uniform porous substrate. Pore level size was used without wettability modification. For spreading diameters, they found that both exponent and prefactor are decreased with increasing porosity. Here, we presented experimental data and analysis for drop spreading in multiscale pores with and without wettability modification.

Biance et al. [1] and Bird et al. [3] gave the following equation for early droplet spreading on solid wall without holes:

$$\frac{D_t}{D_0} = C\left[\frac{t}{\tau}\right]^{\alpha} \tag{2}$$

where C is the prefactor and α is the exponent, τ is the inertia time scale $\tau = \left[\frac{\rho D_0^3}{\sigma}\right]^{0.5}$, here τ equals to 9.85 ms.

Equation (2) was developed based on the assumption that the Laplace pressure is the driving force but the inertia force resists spreading. α equals to 0.5 for complete wetting surface. Following the inertia dominant stage, the spreading diameter obeys the law of $D_t \sim t^{1/10}$ or $D_t \sim t^{1/7}$ for viscosity force dominant spreading [30].

The present problem becomes more complicated due to the non-uniform pore network. In order to understand the viscous force effect on the early spreading, we used the Laplace number as $La = \frac{\rho\sigma D_0}{2\mu^2} \approx 6.9 \times 10^4$ to characterize the importance of surface tension and inertia related to viscosity force. It is shown that the viscosity effect is weak.

Fig. 8 shows non-dimensional spreading diameter D_t/D_0 versus non-dimensional time t/τ. The early inertia dominant spreading still obeys the power law expressed in Eq. (2). The ending of inertia dominant spreading is marked as I. Different samples have different C and α. Now we analyze the effects of pore size, nano-roughness on particle surfaces, and porosity on C and α. Now we analyze the effects of pore size, nano-roughness on particle surfaces, and porosity on C and α. For 556 nm particle sintering material, the pore size is scaled as about 117 nm. Fig. 8b shows that nano-roughness on particle surfaces apparently increases C, compared with smooth particle surface. This is due to the increased wettability by nano-structure modification. α is not influenced by nano-structure. Sintering the nano-particles with Na_2CO_3 pore former generates many pore cavities in the scale of ~10 μm (see Fig. 3). These pore cavities have weak effect on both C and α. Fig. 8d shows C and α for 16 μm particle sintering material. Both nano-roughness on particle surfaces and pore former concentration apparently influence the two parameters. Again, nano-roughness apparently increases C, but have no effect on α. The increase of porosity apparently decreases C and α, which agrees with the numerical findings by Frank and Perre [18] for pore level simulation.

Fig. 8b gave α values in the range of 0.56–0.59 for nano-particle sintering material. Alternatively, Fig. 8d yields α values in the range of 0.49–0.57 for micro-particle sintering material, approaching 0.5 for initial drop spreading on complete wetting surface without holes [1]. This indicates that α is mainly dependent on surface wettability, weakly dependent on the pore network structure. A simple analysis was given here for the nano-roughness effect on initial drop spreading. The wettability of solid surface can be changed by varying free energy or surface micro-structure. The following equation exists [31]:

$$\cos\theta = \frac{\sigma_{gs} - \sigma_{ls}}{\sigma_{gl}} \tag{3}$$

where θ is the contact angle between liquid and solid, the subscripts *g*, *l* and *s* represent gas, liquid and solid, respectively, σ is the surface tension force. If a liquid wets the surface, then $\sigma_{gs} - \sigma_{ls} > 0$. The surface tension force σ_{gs} > 500–5000 mN/m is called high energy surface. Clean copper surface is hydrophilic, for example, having a contact angle of about 80° [32]. Copper oxide (CuO), such as the nano-roughness on particle surface, is super-hydrophilic, for example, having a contact angle of about 30° [33].

For a hydrophilic surface, the surface wettability is enhanced by increasing the surface roughness. The Wenzel model gave [34]:

$$\cos\theta_w = r\cos\theta \tag{4}$$

where θ_w is the contact angle between liquid and micro-structure surface, θ is the contact angle between liquid and smooth surface. We recognize the difference between "actual surface" and "geomet-

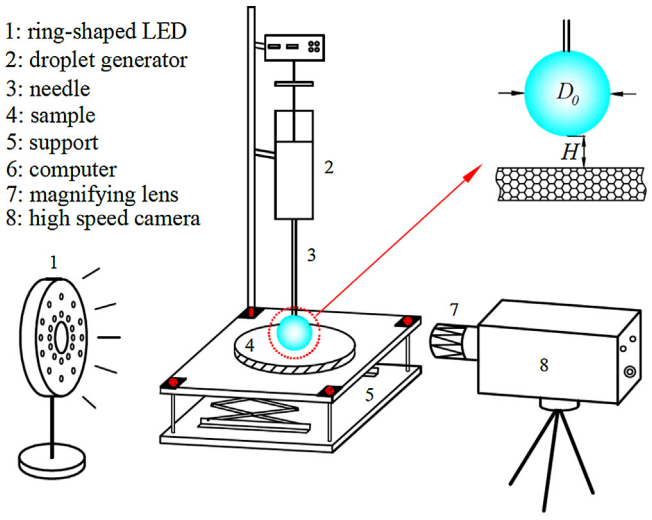

Fig. 4. Experimental setup.

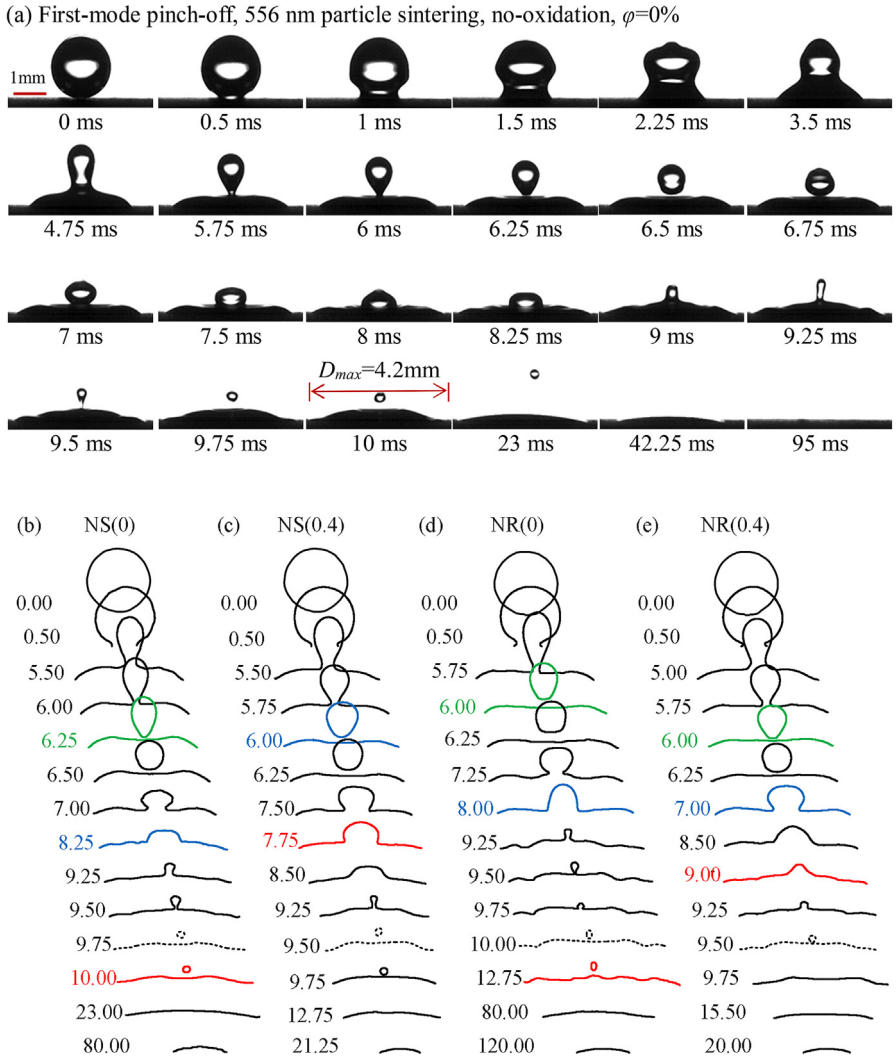

Fig. 5. Sequence video images and shapes for the first mode daughter droplet pinch-off (for NS(0), the first time pinch-off occurs at t = 6.25 ms, the second time pinch-off occurs at t = 9.75 ms).

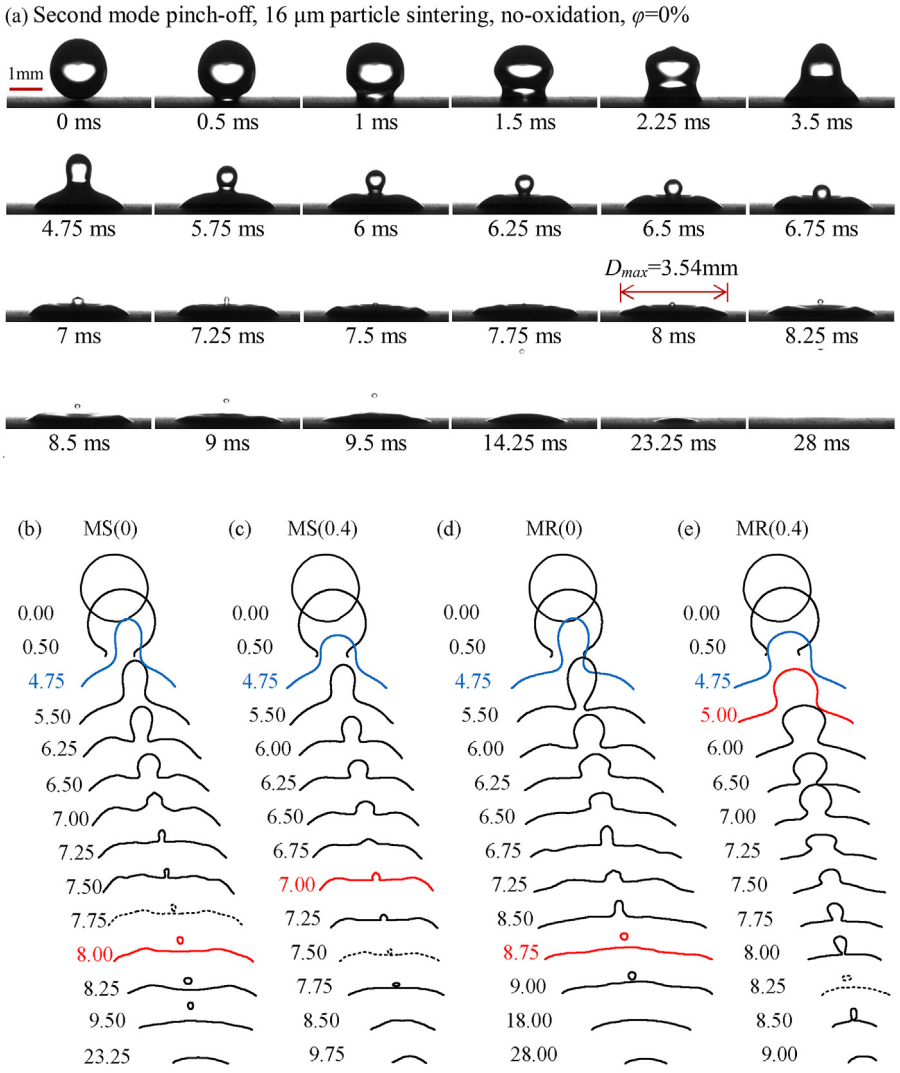

Fig. 6. Sequence video images and shapes for the second mode daughter droplet pinch-off (the first time pinch-off does not happen for all the samples, the second time pinch-off occurs at t = 7.75 ms for MS(0)).

rical surface". Perfect smoothness is an acceptable assumption, as at liquid–liquid or liquid-gas interfaces, actual surface and geometric surface are identical. At any real solid surface, the actual surface will be greater than the geometric surface because of surface roughness. The surface ratio r is termed as the "roughness factor":

$$r = \frac{\text{actual surface}}{\text{geometric surface}} \tag{5}$$

Based on Figs. 1 and 2, r values are roughly estimated to be 1.871 for nano-roughness on 556 nm particle, and 1.872 for nano-roughness on 16 μm particle. The two r values yield the contact angle θ_w of 50.1° for the two cases, showing enhanced hydrophilic behavior, compared with smooth particle. The wettability analysis successfully explains the effect of nano-roughness on particle surfaces on C and α. The nano-roughness enhances wettability to accelerate the early inertia dominant spreading.

3.3. Two modes of daughter droplet emission

We found two modes of daughter droplet ejection. The first mode occurs for the nano-porous substrate, consisting of the first time daughter drop emission during the inertia dominant stage and the second time mini drop ejection during later stage. The second mode refers to the micro-porous substrate, for which the inertia dominant stage does not successfully break up the thick neck, but a second stage still emits a small drop. We explore the connection between the drop spreading on the porous surface and the small drop ejection. In order to do so, the specific time at which various phenomena happen is marked in Fig. 9, in which *FP*, *I*, *SP* and *M* represents the first time daughter drop emission, ending of inertia dominant stage, second time daughter drop generation and maximum spreading diameter.

For nano-porous, the first time drop pinching-off happens during inertia dominant spreading stage. The *FP* points are ahead of *I*, or they occur at the same time, evidencing the close connection between drop ejection and inertia dominant spreading. The second time drop ejection happens either before or beyond the time at the maximum spreading diameter. For micro-porous substrate, the first time drop pinching-off does not occur. The appearance of second time drop ejection is similar to that on nano-porous substrate.

Fig. 10 shows the time at which various phenomena happen. Fig. 10a shows t_{FP} = 6.25 ms for nano-porous samples. The duration time of inertia dominant spreading (t_I) is about 8.25 ms for NS(0) and NR(0). Increase of porosities decreases t_I to be less than 8.0 ms. Maximum spreading diameter occurs at t_M in the range of 7–13 ms. The NR(0) porous had maximum t_M. Nano-roughness on nano-particle surfaces increases viscous resistance for liquid penetration

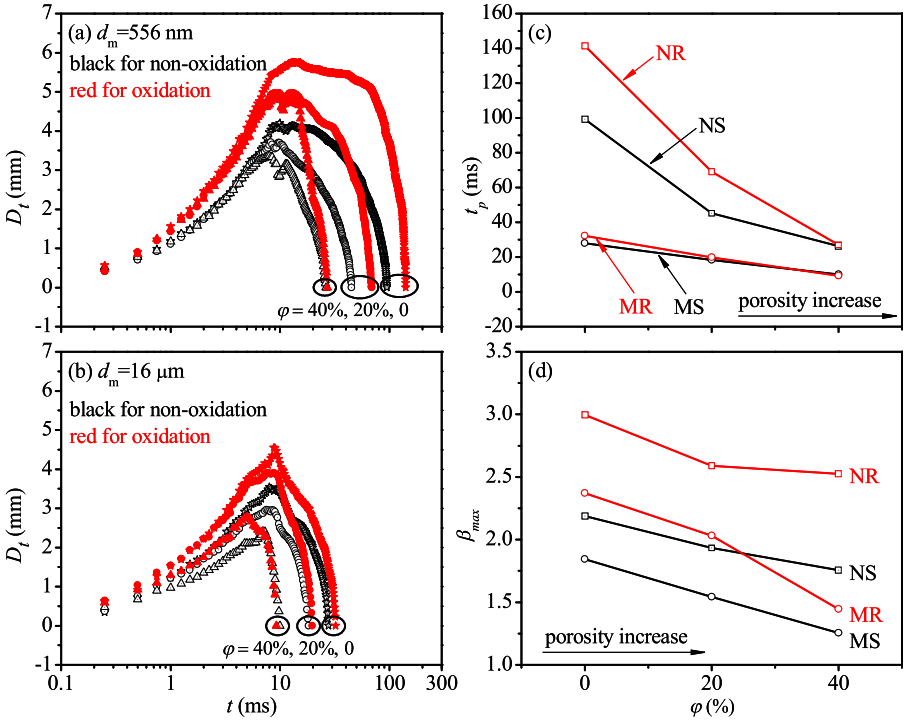

Fig. 7. The drop spreading and penetration dynamics.

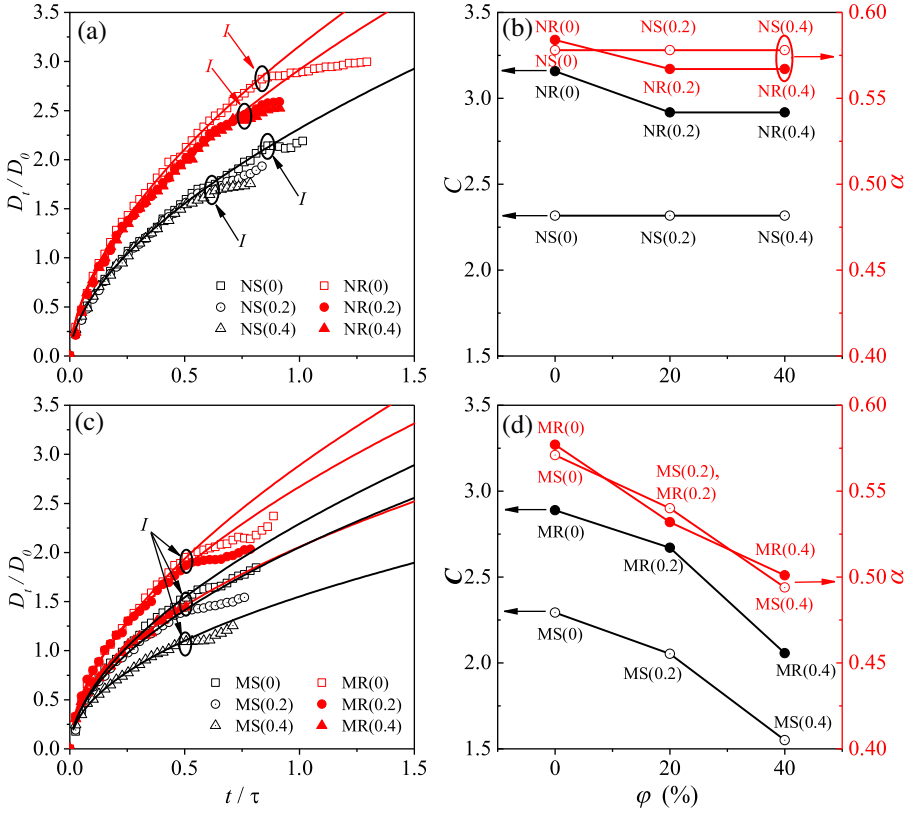

Fig. 8. The early inertial dominant spreading on nano and micro particle sintering porous.

into the porous wick. Besides, the smallest porosity for NR(0) makes the liquid flowing towards the porous wick difficult. Fig. 10a evidences $t_{FP} < t_I < t_M$ for nano-porous. Nano-porous also emits the second time drop, happening either before or beyond the time at the maximum spreading diameter, inferring the second time drop ejection not related to the penetration in porous. The liquid penetration in porous is weaker before t_M and stronger beyond t_M. The micro-porous shortens the inertia dominant spreading lifetime, which becomes 4.25 ms, about 2 ms shorter than nano-porous. Regarding the second time drop ejection time, both nano and micro-porous

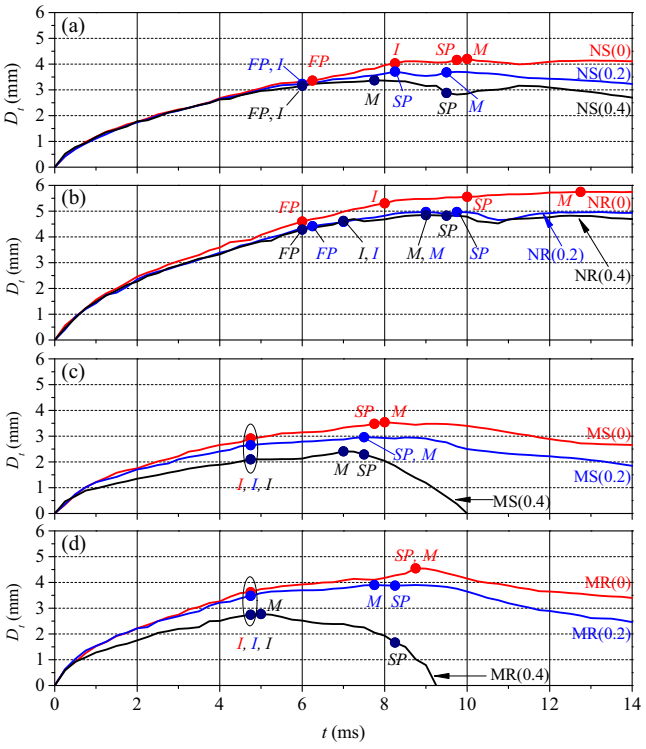

Fig. 9. The dynamic spreading diameters emphasizing sequence of various phenomena (*FP* means the first time daughter drop pinch-off, *I* means inertial dominant spreading, *M* means maximum spreading diameter, *SP* means second time daughter drop pinch-off).

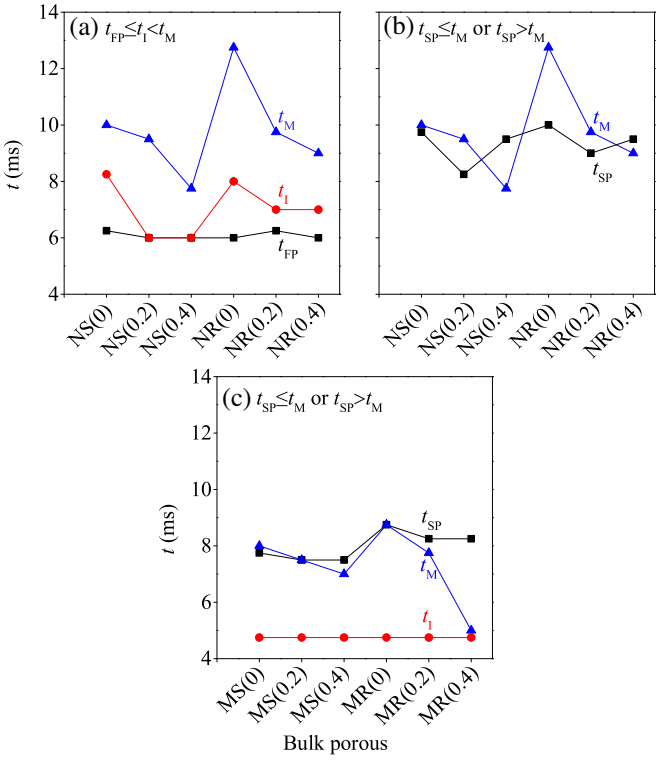

Fig. 10. Effect of particle size, particle surface roughness and porosity on the time at which various phenomena occur (t_{FP} for the first time pinch-off, t_{SP} for the second time pinch-off, t_I for the ending time of inertia dominant spreading and t_M for the time at the maximum spreading diameter).

samples have the relationship of $t_{SP}<t_M$ or $t_{SP}>t_M$. The t_{SP} and t_M curves are intercrossed in Fig. 10b–c.

Figs. 11 and 12 explore the daughter drop pinching-off. In Fig. 11a, images are shown at $t=0.5$ ms, 3.5 ms (almost at maximum H_t) and 6.25 ms (end of inertia dominant spreading) for NS(0). The pinching neck is thoroughly broken up at $t=6.25$ ms. Alternatively, three images are shown for MS(0) in Fig. 11b, identifying the pinching neck diameter of 0.75 mm at $t=4.75$ ms to show no daughter droplet ejection at the end of inertia dominant spreading. Three competitive mechanisms govern if a daughter drop can be successfully ejected. The spreading velocity on the horizontal plane is recorded as $v_{sp}=dD_t/dt$ to lower the pinching neck height h_t. The quick spreading on porous surface causes capillary wave propagation upwards, represented by v_{cw}. The capillary wave starts from

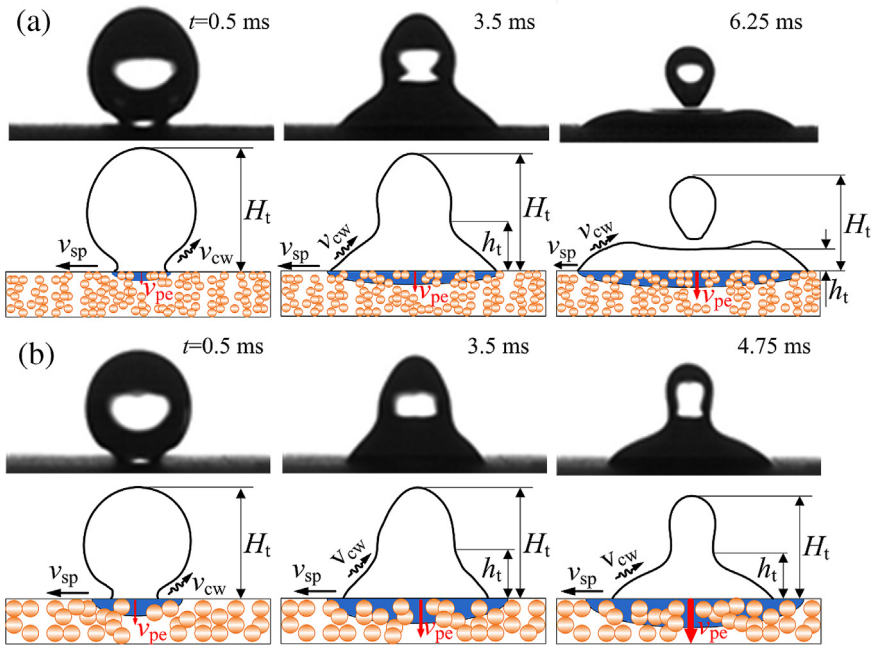

Fig. 11. The daughter droplet pinch-off of NS(0) in a and of MS(0) in b.

the three phase contact point of solid-liquid-gas and propagates along the gas-liquid interface, elevating the pinching neck height h_t. The penetration effect is discussed later.

Fig. 12 shows neck height h_t and drop height H_t, identifying how different mechanisms are competing with each other. It is interesting to find the *S*-shape and double peak distribution of h_t and H_t. The NS(0) and MS(0) porous samples share almost the same $t_{h_t(\max)} \approx 3.5$ms and $t_{H_t(\max)} \approx 4.0$ms. A slight delay of $t_{H_t(\max)}$ than $t_{h_t(\max)}$ is due to the capillary wave traveling from pinching neck to drop top. Three distinct regimes can be divided: regime 1 (competing regime between spreading and capillary wave before $t_{h_t(\max)}$), regime 2 (competing regime among spreading, capillary wave and penetration beyond $t_{h_t(\max)}$), and regime 3 (re-appearance of secondary capillary wave). The h_t curves are inter-crossed for NS(0) and MS(0) substrate. In regime 1, NS(0) has stronger capillary wave effect to elevate h_t compared with MS(0). But in regime 2, NS(0) has faster spreading velocity to lower h_t than MS(0). The re-increase of h_t and H_t for $t > 8$ ms is the evidence of the secondary capillary wave generation. The double h_t peaks correspond to the first and second time daughter drop generation.

The penetration in porous wick has no effect in regime 1, evidenced by identical H_t curves for NS(0) and MS(0) before $t_{h_t(\max)}$. The penetration effect begins to happen for $t > t_{H_t(\max)}$, evidenced by lower H_t curve for MS(0) than NS(0) (see Fig. 12b). The competitive mechanisms determine the inertia dominant spreading lifetime, t_l, and if the first time drop breakup can happen. For nano-porous, t_l is 8.25 ms and lasts until the appearance of the secondary capillary wave. For micro-porous, t_l is shortened to 4.25 ms at which the pinching neck is thick to have a diameter of 0.75 mm (see Fig. 12a). Thus, nano-porous has two times of daughter drop ejections, but micro-porous only has one time drop ejection after the secondary capillary wave.

Fig. 13 summarizes the connection between inertia dominant spreading and daughter drop generation. The connection bridge is the inertia dominant spreading lifetime (t_l). The micro-porous apparently shortens t_l compared with nano-porous. There is enough time to break up the pinching neck for nano-porous, but the time is not sufficient to form thin pinching neck for micro-porous. The second time drop generation mechanism is similar to a drop coalescence with a liquid pool to induce drop bounding [23]. In this work, it is either caused by falling down and re-coalescence of the returned drop with the base drop for nano-porous, or caused by falling down and coalescence of the column-like liquid with the base drop for micro-porous. Both accompany the capillary wave generation.

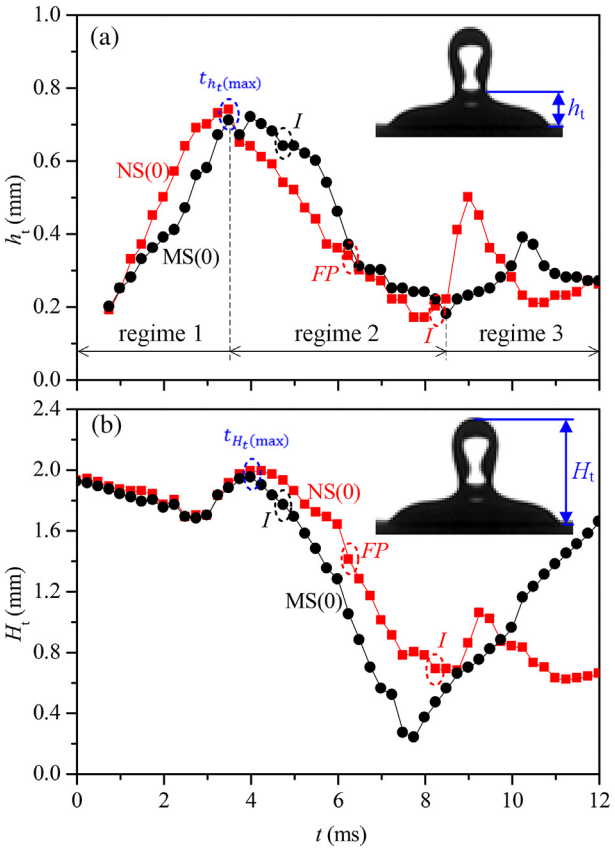

Fig. 12. Droplet height H_t and pinching neck height h_t versus time t (regime 1: competing regime between spreading and capillary wave, regime 2: competing regime among spreading, capillary wave and penetration, regime 3: re-appearance of secondary capillary wave).

3.4. Effect of micro/nano structure on the phenomena

Liquid penetration in porous medium depends on the balance between capillary pressure (driving force) and viscous resistance. Strong conflict exists for liquid penetration in porous medium with

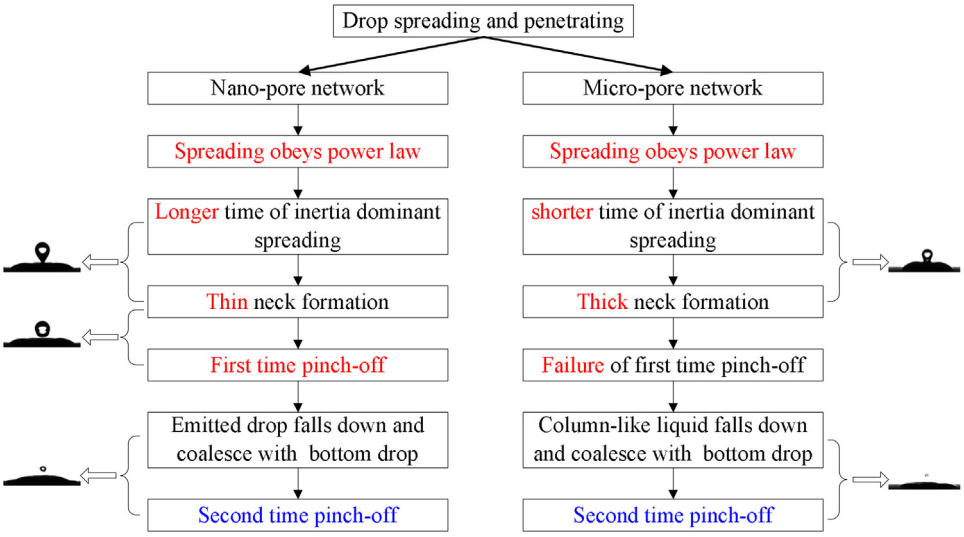

Fig. 13. The logical connection between inertia dominant drop spreading and two modes of daughter droplet emissio.

uniform pores [27]. If one uses smaller pore size, the capillary pressure is larger but the viscous resistance is increased. A larger pore size reduces the resistance but the driving force is smaller. This is the reason why we use multiscale pore network material. The present problem is complicated due to multiscale porous. For porous with smooth particle surfaces, two levels of sizes exist: pore size of $0.21d_p$ and pore channel with its width $\sim d_p$ and length $> d_p$. Three levels of sizes exist for porous with nano-roughness. In case of larger porosity, pore channels are replaced by pore cavities with its diameter in the range of 10–100 μm. The effect of micro/nano structure is summarized as follows.

3.4.1. Effect on inertia dominant spreading (see Fig. 8)

For nano-porous, the nano-roughness on particle surfaces apparently increase C to accelerate spreading, explained by the increased wettability of particle surfaces. The porosity does not change coefficient C and exponent α. For micro-porous, the nano-roughness has similar effect on spreading as to nano-porous. The increased porosity apparently decreases both C and α to slow down spreading.

3.4.2. Effect on the inertia dominant spreading lifetime (see Fig. 10)

The necessary condition for the first time daughter drop ejection is to break up the thin pinching neck during the inertia dominant spreading lifetime. Nano-porous lasts longer duration time thus the ejection is success. Mcro-porous lasts shorter duration time so that such breakup process is failure.

3.4.3. Effect on the penetration time (see Fig. 7)

Penetration time (t_p) characterizes how long is needed for liquid absorption by porous medium. The micro/nano structure strongly influences t_p. Nano-porous lasts much longer t_p than micro-porous. For nano-porous, the increased porosity significantly decreases t_p due to decreased flow resistance by apparent pore channels or pore cavities size. The nano-roughness on nano-particles prolongs t_p due to the increased flow resistance. The micro-porous weakly decreased t_p when the porosity is increased. The nano-roughness has almost no effect on t_p for micro-porous.

3.4.4. Effect on the S-shape pinching neck height (see Fig. 12)

The comprehensive effects of micro/nano structures yield S-shape pinching neck height and double peak distribution. The curves are inter-crossed between nano and micro-porous, indicating different relative importance of three competitive mechanisms. The porous structure has no effect on the secondary drop generation, evidenced by the crossed curves of t_{SP} and t_M in Fig. 10b–c.

4. Conclusions

The conclusions are summarized as follows:

1. Sintering micro/nano particles forms several levels of pore network sizes: pores with diameter of $0.21d_p$, pore channels with width of $\sim d_p$ and length $> d_p$, or pore cavities with diameter of 10–100 μm with pore former involved, and nano-roughness on particle surfaces.
2. Early inertia drop spreading on porous surface follows power law. Nano-roughness increases the surface wettability to increase the coefficient C to speed up spreading for both nano and micro-porous surfaces. The porosity does not change the exponent α for nano-porous. The increased porosity apparently decreases both C and α for micro-porous.
3. Nano-porous lasts longer inertia dominant spreading lifetime, during which the pinching neck is thin and broken up to completely separate the daughter drop from its mother drop (first time daughter drop pinching-off). Micro-porous shortens the duration time. The pinching neck is still thick at the end of the duration time. Thus, the first time daughter drop emission is not success.
4. The necessary condition for the first time daughter drop emission is that if the inertia dominant spreading lifetime is longer enough to completely break up the daughter drop.
5. Comprehensive effects of spreading, capillary wave and penetration yield the S-shape pinching neck height. Three regimes are divided with each having different competition mechanisms. The re-increase of the neck height in regime 3 is the evidence of secondary capillary wave generation, corresponding to the second time daughter drop emission, which is success for both nano and micro-porous.
6. The curves of the secondary daughter drop emission time (t_{SP}) and the time at maximum spreading diameter (t_M) are inter-crossed, indicating the secondary daughter drop production not related to the porous structure.

Acknowledgement

The authors thank for the funding support from Natural Science Foundation of China with contract number of 51436004 and 51210011.

References

[1] A.L. Biance, C. Clanet, D. Quéré, First steps in the spreading of a liquid droplet, Phys. Rev. E 69 (2004) 016301.
[2] R. Rioboo, M.H. Adão, M. Voué, J. De Coninck, Experimental evidence of liquid drop breakup in complete wetting experiments, J. Mater. Sci. 41 (2006) 5068–5080.
[3] J.C. Bird, S. Mandre, H.A. Stone, Short-time dynamics of partial wetting, Phys. Rev. Lett. 100 (2008) 234501.
[4] L. Chen, G.K. Auernhammer, E. Bonaccurso, Short time wetting dynamics on soft surfaces, Soft Matter 7 (2011) 9084–9089.
[5] K.G. Winkels, J.H. Weijs, A. Eddi, J.H. Snoeijer, Initial spreading of low-viscosity drops on partially wetting surfaces, Phys. Rev. E 85 (2012) 055301.
[6] H. Ding, E.Q. Li, F.H. Zhang, Y. Sui, P.D.M. Spelt, S.T. Thoroddsen, Propagation of capillary waves and ejection of small droplets in rapid droplet spreading, J. Fluid Mech. 697 (2012) 92–114.
[7] L. Chen, E. Bonaccurso, M.E. Shanahan, Inertial to viscoelastic transition in early drop spreading on soft surfaces, Langmuir 29 (2013) 1893–1898.
[8] D. Legendre, M. Maglio, Numerical simulation of spreading drops, Colloids Surf. A: Physicochem. Eng. Asp. 432 (2013) 26–33.
[9] R. Sun, H. Bai, J. Ju, L. Jiang, Droplet emission induced by ultrafast spreading on a superhydrophilic surface, Soft Matter 9 (2013) 9285–9289.
[10] S.H. Davis, L.M. Hocking, Spreading and imbibition of viscous liquid on a porous base, Phys. Fluids 11 (1999) 48–57.
[11] S.H. Davis, L.M. Hocking, Spreading and imbibition of viscous liquid on a porous base, II, Phys. Fluids 12 (2000) 1647–1655.
[12] V.M. Starov, S.R. Kosvintsev, V.D. Sobolev, M.G. Velarde, S.A. Zhdanov, Spreading of liquid drops over saturated porous layers, J. Colloid Interface Sci. 246 (2002) 372–379.
[13] V.M. Starov, S.R. Kosvintsev, V.D. Sobolev, M.G. Velarde, S.A. Zhdanov, Spreading of liquid drops over dry porous layers: complete wetting case, J. Colloid Interface Sci. 252 (2002) 397–408.
[14] V.M. Starov, S.A. Zhdanov, M.G. Velarde, Spreading of liquid drops over thick porous layers: complete wetting case, Langmuir 8 (2002) 9744–9750.
[15] A. Clarke, T.D. Blake, K. Carruthers, A. Woodward, Spreading and imbibition of liquid droplets on porous surfaces, Langmuir 18 (2002) 2980–2984.
[16] N. Alleborn, H. Raszillier, Spreading and sorption of a droplet on a porous substrate, J. Colloid Interface Sci. 280 (2004) 449–464.
[17] H. Haidara, B. Lebeau, C. Grzelakowski, L. Vonna, F. Biguenet, L. Vidal, Competitive spreading versus imbibition of polymer liquid drops in nanoporous membranes: scaling behavior with viscosity, Langmuir 24 (2008) 4209–4214.
[18] X. Frank, P. Perré, Droplet spreading on a porous surface: a Lattice Boltzmann study, Phys. Fluids 24 (2012) 042101.
[19] H. Ding, T.G. Theofanous, Propagation of capillary waves and ejection of small droplets in rapid droplet spreading, J. Fluid Mech. 691 (2012) 546–567.
[20] M. Shuai, Y. Rui, J.S. Wu, H. Zhang, Simulation of droplet spreading on porous substrates using smoothed particle hydrodynamics, Int. J. Heat Mass Transf. 77 (2014) 828–833.
[21] X. Frank, P. Perré, H.Z. Li, Lattice Boltzmann investigation of droplet inertial spreading on various porous surfaces, Phys. Rev. E 91 (2015) 052405.

[22] J.B. Lee, D. Derome, J. Carmeliet, Drop impact on natural porous stones, J. Colloid Interface Sci. 469 (2016) 147–156.
[23] F. Blanchette, T.P. Bigioni, Partial coalescence of drops at liquid interfaces, Nat. Phys. 2 (2006) 254–257.
[24] F.H. Zhang, E.Q. Li, S.T. Thoroddsen, Satellite formation during coalescence of unequal size drops, Phys. Rev. Lett. 102 (2009) 104502.
[25] L.H. Tanner, The spreading of silicone oil drops on horizontal surfaces, J. Phys. D: Appl. Phys. 12 (1979) 1473–1482.
[26] Q. Peng, B. Yang, L. Liu, C.J. Song, B. Friedrich, Porous TiAL alloys fabricated by sintering of TiH_2, and AL powder mixtures, J. Alloy. Compd. 656 (2016) 530–538.
[27] X.B. Ji, J.L. Xu, H.C. Li, Y.P. Huang, The decoupling and synergy strategy to construct multiscales from nano to millimeter for heat pipe, Int. J. Heat Mass Transf. 93 (2016) 918–933.
[28] T. Semenic, Y.Y. Lin, I. Catton, Thermophysical properties of biporous heat pipe evaporators, J. Heat Transf. 130 (2008) 022602.
[29] Y.Q. Chen, H.Z. Yu, Q.Y. Zhu, A model of coupled thermosolutal convection and thermoelasticity in soft rocks with consideration of water vapor absorption, Int. J. Heat Mass Transf. 97 (2016) 157–173.
[30] B. Li, P. Somasundaran, P. Patra, Role of self-assembled surfactant structure on the spreading of oil on flat solid surfaces, Adv. Colloid Interface 210 (2014) 72–77.
[31] P.D. Gennes, F. Brochard-Wyard, D. Quere, Capillarity and Wetting Phenomena: Drops, Bubbles, Pearls, Waves, Springer, 2004.
[32] Z.W. He, Z.L. Zhang, J.Y. He, Cuo/Cu based superhydrophobic and self-cleaning surfaces, Scr. Mater. 118 (2016) 60–64.
[33] F. Su, K. Yao, Facile fabrication of superhydrophobic surface with excellent mechanical abrasion and corrosion resistance on copper substrate by a novel method, ACS Appl. Mater. Interface 6 (2014) 8762–8770.
[34] R.N. Wenzel, Resistance of solid surfaces to wetting by water, J. Ind. Eng. Chem. 28 (1936) 988–994.